Chapter 15

Influence of the Synthesis Method on the Preparation Composites Derived from TiO_2-LDH for Phenol Photodegradation

Juan C. Contreras-Ruiz, Sonia Martínez-Gallegos, Jose L. García-Rivas, Julio C. González-Juárez and Eduardo Ordoñez

Additional information is available at the end of the chapter

http://dx.doi.org/10.5772/intechopen.72279

Abstract

Three different TiO_2 catalysts are prepared using different methods. MgAl-CO_3^{2-} layered double hydroxides (LDH) were obtained by the sol-gel method. In the preparation of the composites, the three photocatalysts were combined with LDH following different methodologies. The composites were characterized using X-ray diffraction (XRD), specific surface area (SA), atomic force microscopy (AFM) and X-ray photoelectron spectroscopy (XPS). The influence of the synthesis method on the preparation of the composites was evaluated by analyzing their photocatalytic activity against phenol as a model organic pollutant under UV irradiation. The photocatalytic activity of the composites improves when the chemical interaction, determined by XPS, between the TiO_2 and the LDH decreases. The same happens when the ratio of the anatase-rutile phases, determined by XRD, approaches optimum (80:20%). The effect of the composite concentration in the solution (0.5–2.0 g/L) was investigated, and the light-shielding phenomenon due to high composite concentration decreases the phenol photodegradation. The reduction of photocatalytic activity in reuse cycles is due to loss and partial deactivation of the material. The elimination of phenol is attributed primarily to the photocatalytic process due to the generation of •OH radicals and to a lesser extent the adsorption process also present in the samples.

Keywords: composites, photocatalyst, layered double hydroxides, TiO_2, phenol, degradation

1. Introduction

Synthetic organic composites like phenol are widely used in a great variety of industries including paper, wood, paint, and fertilizers [1]. Wastewater from such industrial processes contains this kind of composite and poses a threat to aquatic life and the environment. It is therefore important to remove or degrade such composites before discharging the wastewater into the environment. Among the technologies used for the degradation of organic pollutants in aqueous media are advanced oxidation processes (AOPs), specifically heterogeneous photocatalysis, which promotes the degradation of several pollutants by broadband semiconductor excitation [2–5]. Photon adsorption by the semiconductor with higher bandgap energy leads to the formation of an electron-hole pair (e^-_{BC}-h^+_{BV}). The photogenerated holes in the valence band are powerful oxidants, while the conduction band electrons are good reducers. The formation of other highly oxidant species (mainly •OH radicals) can also occur; these redox-type reactions occur when the electron-hole recombination is minimized [6]. The use of TiO_2 as photocatalyst has caused great interest due to its high activity, resistance to mild chemical corrosion, low toxicity, and efficiency [7]. The anatase crystalline phase of TiO_2 is more effective than the rutile phase for the photodegradation of several contaminants [5]; however, photoactivity has been found to increase in mixed anatase-rutile phases [8]. One difficulty with the use of TiO_2 is its separation and recovery for possible reuse; the addition of a support material or coadsorbent to immobilize TiO_2 particles to facilitate recycling has been the subject of various investigations [9, 10].

Layered double hydroxides (LDHs) are synthetic composites belonging to the anionic clay family, having a hexagonal or octahedral crystalline structure. They consist of layers of positively charged metal cations, where the surface of the layers is occupied by hydroxyl groups, anions, and water molecules. LDHs are the result of isomorphic variations of brucite-type layers ($Mg(OH)_2$) when Mg^{2+} cations are substituted by Al^{3+} cations, thereby generating a positive charge residue which is offset by the presence of intercalated anions, carbonate (CO_3^{2-}) being the predominant anion [11]. Hydrotalcite is an LDH-type layered material, with the chemical formula $[M^{2+}_{1-x}M^{3+}_x(OH)_2]_x(A^{n-})_{x/n} \bullet mH_2O$, where M^{2+} and M^{3+} are di- and trivalent cations (Mg^{2+} and Al^{3+}) and A^{n-} is the intercalated anion. LDH and its calcined products are porous materials with large surface area, have the capacity to adsorb pollutants, and have proven suitable for immobilizing TiO_2 particles for the photodegradation of organic pollutants [12, 13].

The aim of this work is to synthesize composites derived from the TiO_2 photocatalyst and the LDH anionic clays to study the influence of the preparation method on the photocatalytic capacity of those composites in a phenol solution. Two groups of synthesis methods were used: the first one is to obtain the TiO_2 photocatalyst, and the second one is in the preparation of the TiO_2-LDH composites. The LDH was prepared by the sol-gel method, according to previously optimized procedures [14, 15] in relation to its photoactivity evaluated with the degradation of phenol. The synthesized composites in this work were also tested for phenol photodegradation in aqueous solution. These materials also showed advantages in their reusability and were able to be used in four photocatalytic cycles with a minimum loss in the photocatalytic activity at the end of the test.

http://dx.doi.org/10.5772/intechopen.72279

2. Materials and methods

2.1. TiO_2 synthesis

The photocatalysts were synthesized using three methods. (i) First, following the sol–gel procedure [16], 5.25 mL of titanium isopropoxide (TTIP) $Ti[OCH(CH_3)_2]_4$ were added to 97% (Sigma-Aldrich) in 47 mL of ethanol (Civeq); the mixture was agitated for 3 hours after which 12.25 mL of deionized water were added. Agitation continued at 78°C for 20 hours. The solid was washed with deionized water by centrifugation and dried at 80°C during 1 hour. The resulting powder was ground and calcined (TiO_2I). (ii) In the second method, 90 mL of 1-butanol $C_4H_{10}O$ (Sigma-Aldrich) were mixed with 120 mL of deionized water; both reagents were heated at 70°C in a water bath with continuous agitation and reflux system. Subsequently, 45 mL of titanium butoxide (TOBT) $C_{16}H_{36}O_4Ti$ 97% (Sigma-Aldrich) were added by dripping. The mixture was aged during 24 hours at constant agitation and temperature. The resulting solid was recovered and washed by centrifugation using ethanol, dried during 24 hours at 100°C, and finally calcined (TiO_2B). (iii) The third method of obtaining TiO_2 was direct calcination of TTIP by placing 10 mL in mechanical agitation in air for 30 minutes, before being calcined (TiO_2T). In all cases, calcination took place at 550°C for 3.5 hours.

2.2. LDH synthesis

LDHs were synthesized by the sol–gel method [17], mixing 5.72 g of magnesium ethoxide $C_4H_{10}MgO_2$ (Aldrich) in 100 mL of ethanol CH_3CH_2OH (99.5%) (Civeq) and adding 8.8 mL of HCl (Fermont); the mixture was maintained at 80°C with reflux and agitation. The second solution was prepared by dissolving 5.4 g of aluminum acetylacetonate $C_{15}H_{21}AlO_6$ (Aldrich) in 80 mL of ethanol and added dropwise to the first solution maintaining pH 10 with a 3:1 solution of NH_4OH in water. The mixture was aged for 20 hours. The solid was separated by centrifugation and dried at 100°C for 24 hours (LDH). It was then calcined at 550°C for 3.5 hours (CLDH).

2.3. Synthesis of TiO_2-LDH composites

As previously reported, in the preparation of HDL-TiO_2 composites [15], the use of anionic clays synthesized by the sol-gel method has advantages over those prepared by the conventional coprecipitation method, because the sol-gel HDL possesses smaller crystal size, which offers a bigger dispersion of TiO_2 particles on the surface of material minimizing the photocatalyst screening phenomenon. In this work according to previous tests, three methodologies were chosen in the preparation of composites derived from TiO_2 and sol-gel HDL based on their photocatalytic efficiency, which are representative for the three different synthesized photocatalysts:

(i) In the first method, 2.0 g of TiO_2I catalyst were mixed with the gel during LDH synthesis, continuing with the methodology described in the previous paragraph. Finally, the solid was calcined at 550°C for 3.5 hours (TiO_2I-LDH).

(ii) In the second method, 2.0 g of the TiO_2B catalyst and 0.2 g of the CLDH solid were mixed in 20 mL of ethanol with mechanical agitation for 3 hours; the resulting paste was dried at 100°C for 20 hours (TiO_2B-LDH).

(iii) In the preparation of the third composite, 9 mL of TTIP were mixed with 0.5 g of CLDH, and the mixture agitated for 30 minutes in the air. The samples were then calcined at 550°C for 3.5 hours (TiO_2T-LDH). **Figure 1** illustrates the processes described above in the preparation of TiO_2-LDH composites.

2.4. Characterization

The materials obtained were characterized by XRD using Siemens D500 diffractometer (Cu kα λ = 1.54 Å) at a scanning speed of 2(°2θ)/min. The specific surface area was determined by N_2 adsorption using the BET method on BELSORP-max equipment. The surface analysis of the materials by the AFM technique was performed in an Oxford Asylum Research Cipher AFM at room conditions with noncontact mode with a Si tip of 10 nm radius and resonance frequencies from 180 to 240 kHz. The measurements were taken in a range of 500 × 500 nm. The composites were also analyzed by XPS using Thermo Scientific K-Alpha X-ray photoelectron spectrometer, using the Al kα radiation line (1487 eV) in standard mode, with 10 scans, tip size of 400 μm, step voltage of 200.0 eV, and pass energy of 1.0 eV. All the characterization analysis was performed prior to the photocatalytic tests.

2.5. Phenol photodegradation and adsorption tests

The LDH, CLDH, TiO_2I, TiO_2B, and TiO_2T precursors and TiO_2I-LDH, TiO_2B-LDH, and TiO_2T-LDH composites were mixed separately with a phenol solution (Baker) (C_0 = 10 mg/L). Air was pumped through each mixture to maintain constant agitation, and the solution was stabilized for 20 minutes. Three different conditions were evaluated: (i) under UV light with a UVS-18 EL (λ = 264 nm, 8 w) lamp and in the absence of solid (photolysis), (ii) in the dark without UV irradiation and with the synthesized materials (adsorption), and (iii) under UV light with the presence of the synthesized solids (photocatalysis). The experiments were conducted for 120 minutes at room temperature (20°C) and without external pH variation. The effect of different concentrations of the prepared composites was also evaluated at concentrations of 0.5, 1.0, 1.5, and 2.0 g/L; aliquots were extracted at 0, 5, 10, 30, 50, 80, and 120 minutes during

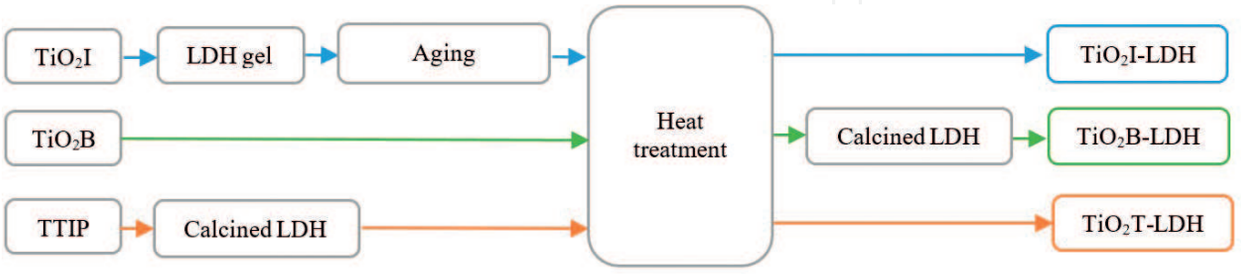

Figure 1. Methodologies for TiO_2-LDH composite preparation.

the experiments. The phenol concentration was determined by UV-Vis spectrophotometry using the 4-aminoantipyrine method [18]. In order to determine the reuse capacity of the synthesized composites, photodegradation tests were conducted with UV irradiation using the same solid in consecutive rounds. At the end of a photodegradation cycle, the material was recovered from the solution by sedimentation and reused with a new phenol solution until four cycles were completed.

3. Results and discussion

3.1. Characterization

Figure 2 shows the X-ray diffraction patterns for the synthesized TiO_2 precursors along with the LDH and its calcined product CLDH. For the photocatalysts, the TiO_2I sample is composed mostly of the crystalline structure related to the TiO_2 anatase phase, presenting peaks at 25.4, 37.9, 48.1, 54.1, 55.2, and 62.6 °2θ (JCPDS 01-089-4921), in addition to a peak related to the TiO_2 brookite phase at 30.9 °2θ (JCPDS 00-029-1360). The diffractogram for the TiO_2T sample shows a bigger variety in the different crystalline structures that this photocatalyst possesses, with a main peak at 25.4 °2θ and smaller peaks at 37.9, 48.1, 54.0, and 55.2 °2θ referring to the TiO_2 anatase phase (JCPDS 01-089-4921). In smaller proportion characteristic, reflections of the TiO_2 phase with rhombohedral structure are observed in 32.9, 35.7, and 40.8 °2θ (JCPDS 01-071-0146), a peak at 43.7 °2θ of TiO with monoclinic structure (JCPDS 01-072-0020) and one lower peak associated with TiO_2 rutile phase with tetragonal coordination at 27.6 °2θ (JCPDS 01-089-4920). The TiO_2B sample shows peaks referring to the TiO_2 anatase phase at 25.4, 37.9, 48.1, 54.0, and 55.2 °2θ (JCPDS 01-089-4921) and a signal at 30.9 °2θ of the TiO_2 brookite with orthorhombic crystalline formation (JCPDS 00-029-1360), as well as peaks related to the TiO_2 rutile phase at 27.6 and 36.2 °2Θ (JCPDS 01-089-4920).

In a photocatalyst, the pure anatase phase is considered photocatalytically superior to the rutile phase, which, although more heat stable, at the same time has a higher rate of electron–hole recombination (e^-_{BC}-h^+_{BV}) and a lesser affinity for the adsorption of organic compounds like phenol [19]. A key factor in the photocatalytic activity of TiO_2 is to obtain a mixed anatase-rutile material at an optimal ratio of about 80:20%, which has lower recombination rates (e^-_{BC}-h^+_{BV}) due to the interconnection of the electronic bands, in which the rutile phase acts as e^-_{BC} collector. In the meanwhile, the anatase phase is the photocatalytically active part causing oxidation and reducing reactions, which are carried out separately, maximizing the photocatalytic mechanism [8]. The composition of the precursor photocatalysts in the anatase-rutile phases was determined by the Spurrs and Myers equation [20], finding that the optimal anatase-rutile phase ratio (80:20%) was close to be found in samples TiO_2T (82:18%) and TiO_2B (89:11%). Meanwhile, the rutile phase of TiO_2 was not observed in the TiO_2I photocatalyst; only the anatase and brookite phases were present. These results occasionally influence the performance of these materials and the composites used in the photocatalytic tests, as discussed later.

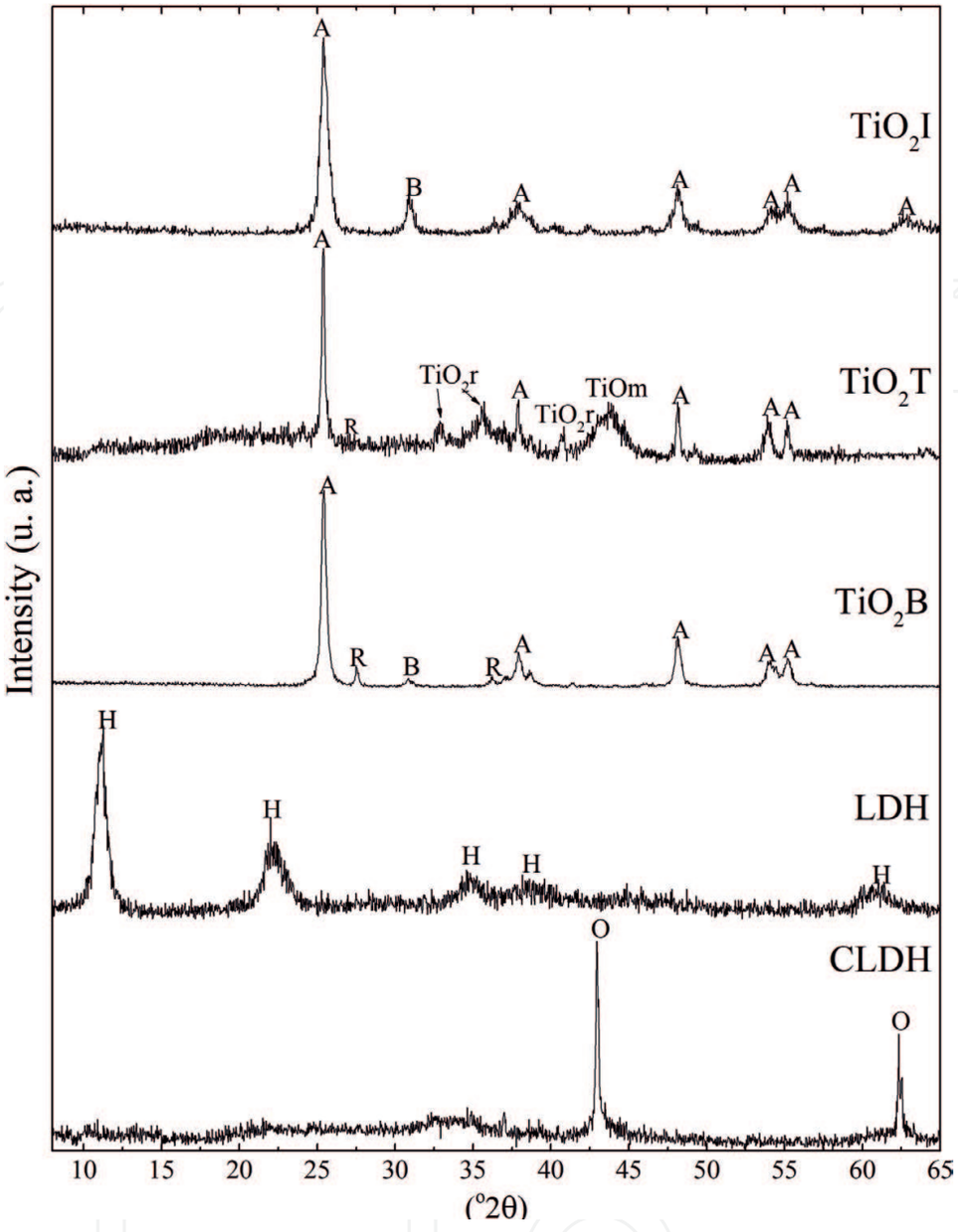

Figure 2. XRD patterns for TiO_2 and LDH compounds, with A (TiO_2 anatase), R (TiO_2 rutile), TiO m (TiO monoclinic crystalline structure), TiO_2 r (TiO_2 rombohedric crystalline structure), B (TiO_2 brookite) H (LDH), and O (MgO) peaks.

The diffraction pattern of LDH (**Figure 2**) shows the typical rhombohedral structure of an MgAl layered double hydroxide, where the diffraction at 11.3 °2θ corresponds to the basal plane (003), defined as the distance between two adjacent layers. Harmonic reflections corresponding to planes (006), (009), (012), (015), and (110) can also be observed at 22.0, 34.6, 38.2, 47.8, and 61.0 °2θ, respectively (JCPDS 00-014-0191) [21]. The diffraction pattern for CLDH (**Figure 2**) shows the characteristic peaks of periclase MgO with crystallographic planes (200) and (220) at 42.9 and 62.3 °2θ, respectively (JCPDS 00-003-0998), which correspond to crystals of a MgAl mixed oxide associated with the collapse of the laminar structure of the LDH [21, 22].

Figure 3 shows the X-ray diffraction patterns for the synthesized TiO_2-LDH composites. In the case of the TiO_2T-LDH composite, the TiO_2 anatase phase and the mixed oxides can be observed separately; the reflections of the TiO_2 anatase phase are predominant at 25.4, 37.0, 37.9, 48.1, 54.0, and 55.2 °2θ (JCPDS 01-089-4921). A less intense peak can be seen at 42.9 °2Θ (JCPDS 01-003-0998) corresponding to CLDH component and another peak at 32.9 °2θ of the MgTi mixed oxide with rhombohedral crystalline structure (JCPDS 01-079-0831), thus confirming the immobilization of TiO_2 in the composite through the calcination process and achieving the diffusion of the photocatalyst in the composite [21, 23].

The TiO_2I-LDH composite mostly shows diffraction of the $MgTiO_3$ mixed oxide with rhombohedral structure, with a main peak located at 32.9 °2θ and secondary peaks at 19.3, 21.3, 24.1, 35.7, 40.8, 49.3, 53.7, 62.1, and 63.8 °2θ (JCPDS 01-079-0831). The crystal structure of monoclinic TiO presents two diffractions with peaks located at 42.1 and 43.1 °2θ (JCPDS

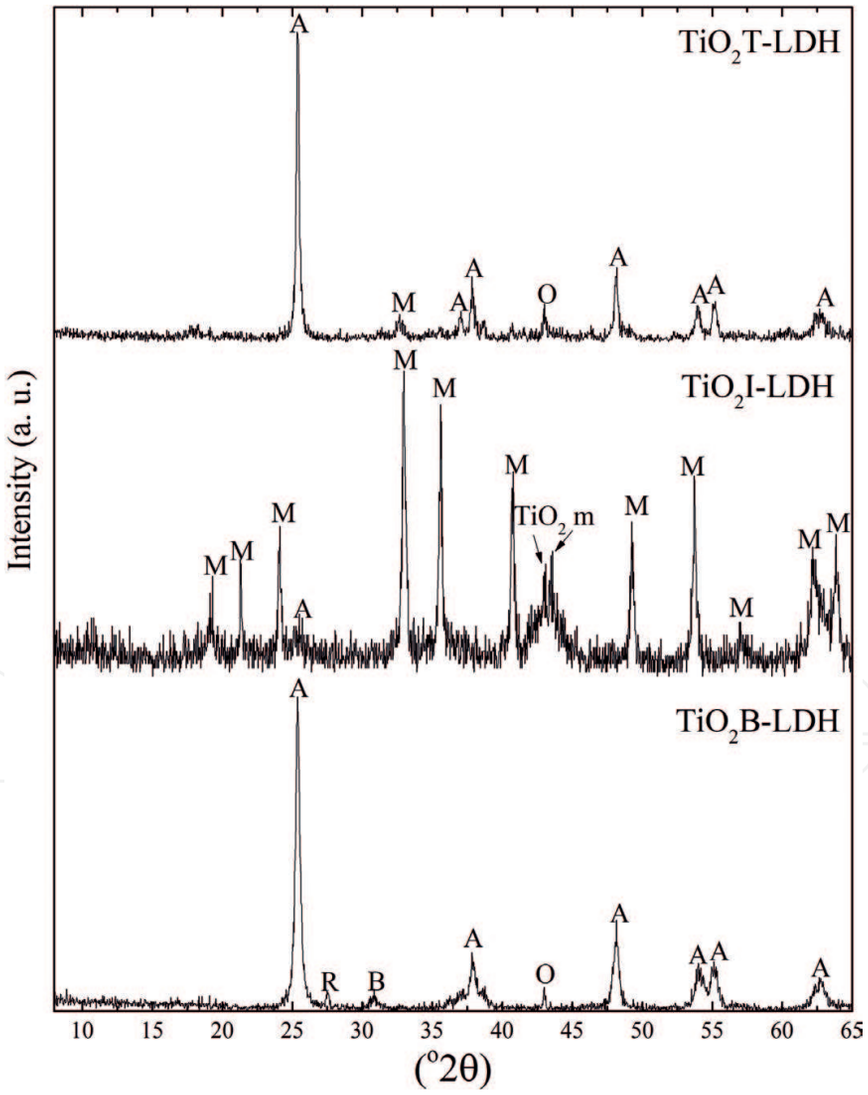

Figure 3. XRD patterns for TiO_2 and LDH compounds, with A (TiO_2 anatase), R (TiO_2 rutile), TiO_2m (TiO_2 monoclinic crystalline structure), B (TiO_2 brookite), O (MgO), and M ($MgTiO_3$ rombohedric crystalline structure) peaks.

01-072-0020). The TiO_2 anatase phase in this composite is seen in a small peak of (110) plane at 25.4 °2θ (JCPDS 01-089-4921) suggesting that only a small part of Ti exists in this phase and the rest is dispersed over the MgAl mixed oxide [21]. Supporting the above statement, no diffraction spikes attributed to the MgAl mixed oxide can be observed, suggesting that the impregnated TiO_2 particles are disaggregated [24] when mixed with the LDH gel and prior to the heat treatment of the composite, achieving a chemical interaction between the composites resulting in the formation of the $MgTiO_3$ phase [25].

The diffraction pattern of the TiO_2B-LDH composite is mostly composed of diffractions with the TiO_2 anatase phase at 25.4, 37.9, 48.1, 54.1, 55.2, and 62.6 °2θ (JCPDS 01-089-4921); similarly, it is possible to observe a peak relating to the TiO_2 rutile phase at 27.6 °2θ (JCPDS 01-089-4920), a signal at 30.9 °2θ of the TiO_2 brookite phase (JCPDS 00-029-1360), and a lesser intense peak at 42.9 °2θ associated with the MgO oxide (JCPDS 00-003-0998). Reflections related to the formation of $MgTiO_3$ mixed oxide are absent.

These results confirm the addition of TiO_2 in the composites. In the case of TiO_2I-LDH, there are significant changes in the structure with respect to the precursors, whereas in the TiO_2T-LDH and TiO_2B-LDH samples, the components remain segregated.

Properties such as the photocatalytic crystalline phases, the proportion of each one, and the size of the crystals in photocatalysts are influential in the generation and/or recombination of electron–hole pairs. The formation of the different crystalline phases of a photocatalyst is related to the atomic arrangement and the facet that shows the crystals during irradiation in photocatalytic processes [16]. The crystal sizes of the synthesized samples are calculated using the Debye-Scherrer equation [26] and are given in **Table 1**. The preparation temperature on TiO_2 synthesis affects the formation of the anatase and rutile phases, which is reflected in the size of the crystal formed [27]. The crystal size for the composites is from 26 to 36 nm, observing that the different methodologies used to prepare the composites influence the size of the crystals formed. The TiO_2T-LDH and TiO_2B-LDH composites present a similar crystal size to the TiO_2T and TiO_2B photocatalysts, while the crystal size for TiO_2I-LDH

Sample	Crystal size (nm)	AS_{BET} (m^2/g)	Total pore volume (cm^3/g)	Average pore diameter (nm)
TiO_2T	34	1.48	0.003	8.16
TiO_2I	16	62.99	0.180	11.40
TiO_2B	25	54.61	0.113	8.30
LDH	11	87.09	0.169	7.74
CLDH	43	77.47	0.151	7.80
TiO_2T-LDH	36	70.44	0.175	9.95
TiO_2I-LDH	31	90.12	0.239	10.61
TiO_2B-LDH	26	45.29	0.111	9.82

Table 1. Crystal size and textural characteristics of the composites.

is almost double that the TiO_2I sample. Similarly, the generation of nanometric crystals in LDH (11 and 43 nm of LDH and CLDH, respectively) that are obtained by sol-gel synthesis may enable a more homogeneous interaction with TiO_2 compared to other methods of LDH synthesis [28–29].

The textural properties of a photocatalyst affect its contact with pollutants. The heterogeneous photocatalysis process performs better in photocatalysts with high surface area, which increases the probability that the molecules of the pollutant and its oxidation intermediates are in direct contact with the photogenerated holes during irradiation, thus enhancing the photodegradation process [19].

Table 1 shows the results of surface area, total volume, and mean pore diameter of the synthesized solids. The mean diameter of the samples is in the range of 2 to 50 nm assigning them mesoporous materials [22]. The N_2 adsorption-desorption isotherms that were obtained for the materials in all cases were type IV according to IUPAC classification, where a slow increase in the adsorption process can be observed, followed by a rapid adsorption typical of mesoporous materials. Furthermore, the hysteresis loop for all materials correspond to H3 type, which is associated with the filling and emptying of the mesopore by capillary condensation; this type of hysteresis is usually found in materials that form particle aggregates, which indicate the presence of asymmetric pores, with nonuniform size and shape [4, 30]. In the prepared composites, the presence of TiO_2 induces profound changes in the textural properties of the solids; TiO_2I-LDH presents a bigger surface area (90.12 m^2/g) compared to the TiO_2I and LDH precursors (62.99 and 77.47 m^2/g, respectively), attributed to the increase of the pore volume in samples [4]. The preparation of this composite entirely by a sol–gel route also accounts for the greater specific surface area of this sample. This behavior is not observed in TiO_2T-LDH, since it has a smaller surface area (70.44 m^2/g), attributed to the contribution of the surface area of the photocatalyst TiO_2T used as precursor (1.48 m^2/g), whereas the surface area for TiO_2B-LDH is reduced (45.29 m^2/g) compared to the TiO_2B precursors and calcined LDH (54.61 and 77.47 m^2/g, respectively), attributed to the reduced number of accessible pores, reflected in a slight reduction in pore volume [24].

The AFM characterization in noncontact mode of TiO_2 and CLDH precursors and the composites obtained is shown in the images in **Figure 4**. The surface morphology observed in the two- and three-dimensional (2D and 3D) images for the TiO_2T photocatalyst consists of spherical particle agglomerates with diameters in the range of 35 to 175 nm. As can be seen in the images, the particles for TiO_2I and TiO_2B precursors preserve their shape, while their size decreases considerably to diameters in the range of 15 to 50 nm as a result of the sol-gel process used to synthesize these two photocatalysts in particular [31], which is related to the crystal size obtained for these materials. The image for CLDH shows a topography formed by densely packed plate-shaped particles whose horizontal dimensions vary from 40 to 100 nm.

On the other hand, in the TiO_2T-LDH composites, a more uniform morphology can be seen on comparing TiO_2I-LDH and TiO_2B-LDH, where in the latter, it can be more clearly appreciated how the components contrast where the smaller spherical particles of TiO_2 are spread over the surface of the larger plates of the LDH component, thus confirming the formation of the composites.

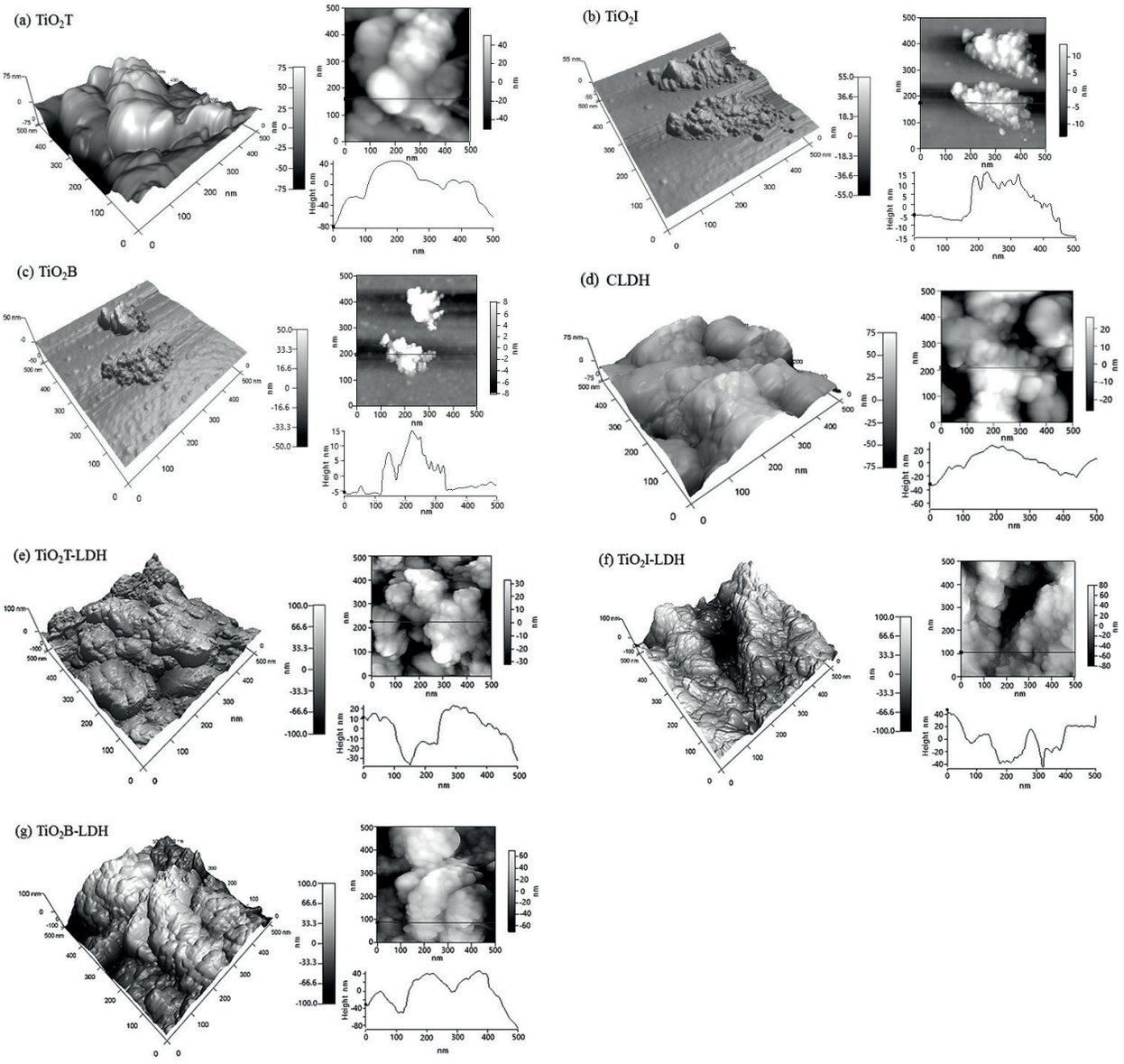

Figure 4. AFM 3D–2D images and height profiles for (a) TiO_2T, (b) TiO_2I, (c) TiO_2B, and (d) CLDH samples and (e) TiO_2T-LDH, (f) TiO_2I-LDH, and (g) TiO_2B-LDH composites.

Surface roughness can be quantitatively identified using the data obtained from the AFM analysis through the definition of the quadratic mean, as follows [32]:

$$R_{rms} = \sqrt{\frac{\sum_{n=1}^{N}(z_n - z)^2}{N-1}} \quad (1)$$

where R_{rms} is the roughness of the mean quadratic value, z_n is the height of the n_{th} data point, z is equal to the average height of the z_n values obtained by AFM topography, and N is the number of data points. The results of statistical analysis for the materials used are shown in **Table 2**.

Muestra	TiO_2T	TiO_2I	TiO_2B	CLDH	TiO_2T-LDH	TiO_2I-LDH	TiO_2B-LDH
R_{rms} (nm)	32.54	6.72	4.56	18.44	18.75	40.84	39.71

Table 2. Roughness values of quadratic mean (R_{rms}) for the precursors and synthesized composites.

As observed in the surface profiles in **Figure 4**, all the samples presented roughness, the TiO_2T photocatalysts having a higher value compared to the TiO_2I and TiO_2B precursors. This trend coincides with the reduced particle size observed for these last photocatalysts, whereas the CLDH precursor presents a roughness with intermediate value compared to that obtained in the photocatalysts. The TiO_2T-LDH composite shows a decrease in the R_{rms} value compared to the value of TiO_2T; a reduction in the roughness value is representative of the homogeneity of the particles [33], suggesting that the photocatalyst is diffused inside the composite, while the surface is constituted mostly by the CLDH component. This result is not observed in the AFM images for the TiO_2I-LDH and TiO_2B-LDH composites, indicating that in these materials the photocatalyst remains more superficially exposed.

The high-resolution XPS spectra for the O 1 s and Ti 2p regions of the TiO_2-LDH composites are presented in **Figure 5**. The O 1 s spectra signals for the TiO_2T-LDH material decompose into energy peaks at 529.48, 530.01, 531.77, and 532.87 eV attributed to the bonds in TiO_2, MgO, Al_2O_3, and CO, whereas the Ti 2p spectrum is resolved in the coordinations that form the Ti in Ti_2O_3 and TiO_2 (octahedral coordination) and the TiO_2/Al_2O_3 interaction, which are related to the binding energies 456.90, 458.15, and 458.89 eV, respectively [21, 34].

The XPS O 1 s spectrum for TiO_2I-LDH is resolved in spikes with binding energies of 529.66, 530.43, 532.10, and 533.37 eV which correspond to TiO_2, MgO, Al_2O_3, and CO composites. The resolution of the XPS spectrum of Ti 2p3/2 region shows spikes with binding energies of 456.93, 458.34, and 459.05 eV corresponding to Ti_2O_3 and TiO_2 (octahedral) and TiO_2/Al_2O_3; this latter as a result of the chemical interaction between the LDH oxides and the impregnated TiO_2 [12, 30, 34].

The resolution of the XPS spectra for the TiO_2B-LDH composite in the O 1 s region shows the contributions of O forming bonds in the MgO, TiO_2, Al_2O_3, and CO composites with peaks at 529.20, 529.99, 531.80, and 532.75 eV, respectively. The binding energies of the Ti 2p3/2 region found at 457.34, 458.74, and 460.34 eV indicate their presence forming the Ti_2O_3, TiO_2 (octahedral), and TiO_x (tetragonal) composites, respectively [29, 34].

Similarly, in the XPS spectra of **Figure 5** corresponding to the Ti 2p region, a traditional Ti 2p spectrum can be observed, where the intensity of the Ti 2p3/2 peak is higher than for the Ti 2p1/2 peak. It can also be seen that in all the composites the neighboring distances between the main Ti 2p3/2 and Ti 2p1/2 peaks are close to 5.9+/−0.2 eV. This value indicates that the charged TiO_2 particles in the composite have an octahedral coordination typical of the anatase phase [12, 21, 35].

The XPS analysis shows the different types of Ti coordination in the samples; the octahedral TiO_2 coordination is predominant in all the samples. The chemical interaction of Ti with the

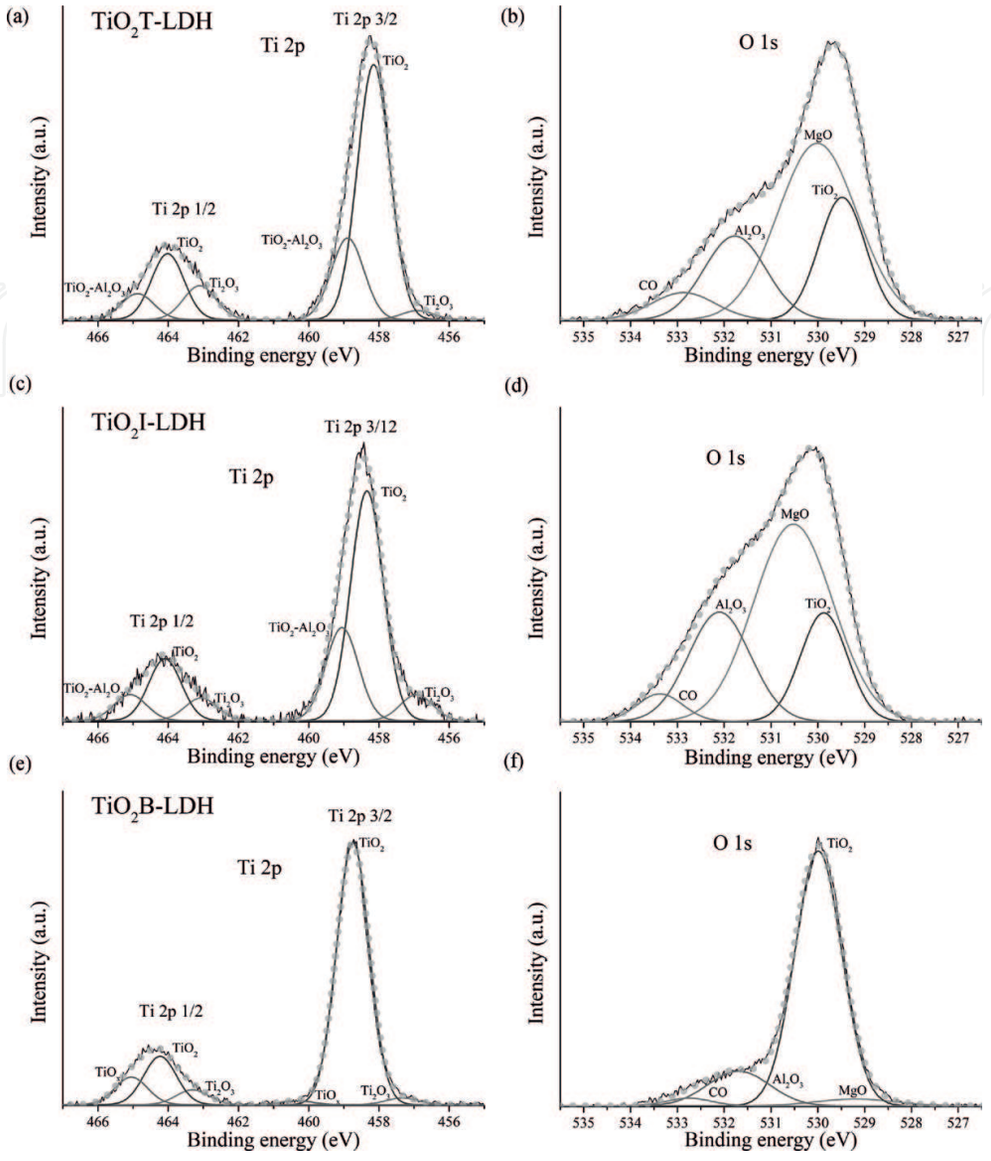

Figure 5. XPS spectra for Ti 2p and O 1s regions for TiO_2-LDH composites.

LDH also presents [12]. From these results, it can be deduced that the composites obtained are not mixtures of unrelated components, rather than there is a chemical interaction between them. According to the literature [36], chemical interaction reduces photocatalytic efficiency since the Ti is incorporated into the structure, remaining a lesser extent on the surface. This occurs with greater frequency in the TiO_2I-LDH composite where, based on the different Ti coordinations presented (see **Figure 6**), the chemical bond between the TiO_2-Al_2O_3 components occurs in 25.9%, whereas this contribution is lower (19.6%) for TiO_2T-LDH and is not observed in TiO_2B-LDH. However, TiO_2B-LDH is possible to observe the tetragonal TiOx coordination which may enhance photocatalytic efficiency in the degradation of phenolic composites [21], directly relating these results to the photocatalytic degradation rates of each of these materials as it is shown below.

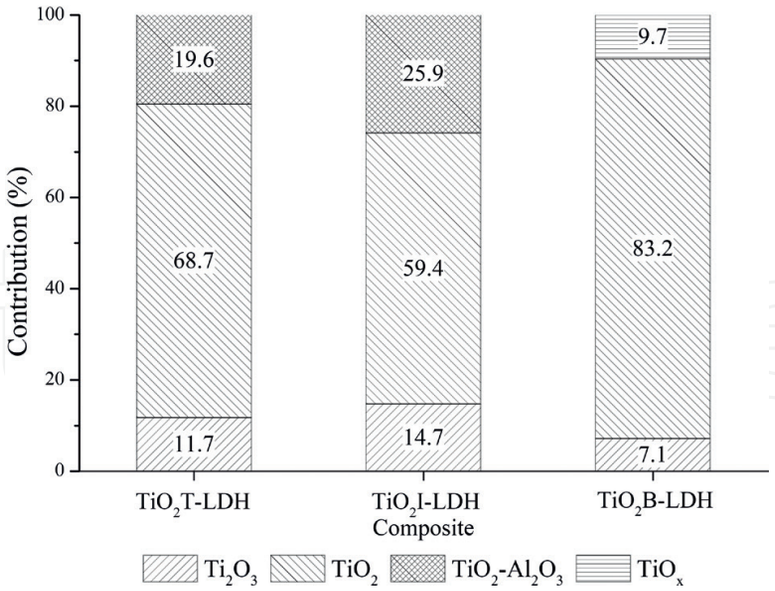

Figure 6. Contributions of Ti coordinations in TiO_2-LDH composites.

Muestra	Mg	Al	Ti	C	O	Ti/(Mg + Al)
TiO_2T-LDH	14.95	6.83	9.83	24.01	44.38	0.45
TiO_2I-LDH	30.54	10.06	5.31	9.11	44.98	0.13
TiO_2B-LDH	9.74	0.95	15.29	22.40	51.62	1.44

Table 3. Elemental analysis by XPS (% atom.) and relation Ti/(Mg+Al) for TiO_2-LDH composites.

The elementary XPS study in terms of atomic percentage produces the results shown in **Table 3**. The presence of Ti in the composites is lower in TiO_2I-LDH, leading us to say that the methodology used in the preparation of this composite is not conducive to its incorporation on the surface, while for TiO_2T-LDH and TiO_2B-LDH, the percentage of surface Ti is higher (9.83 and 15.29%, respectively).

The loading of TiO_2 over the LDH surface can be determined by means of the Ti/(Mg + Al) ratio [36] through elementary XPS analysis, finding values of 1.44, 0.45, and 0.13 for TiO_2B-LDH, TiO_2T-LDH, and TiO_2I-LDH, respectively. The results are attributed to the synthesis methods used in the preparation of the materials, finding that the direct mixing of the TiO_2 and LDH solids as in TiO_2B-LDH leads to a lower Ti propagation inside this composite, enabling increased activity per unit of mass, reducing the agglomeration of photocatalytically active particles and the screening phenomenon, as well as allowing the easy separation and recovery of the solid at the end of its use in photocatalytic processes [36]. Contrary to the aforementioned, the TiO_2I-LDH sample presents a lower value in Ti loading, attributed to the direct mixing of the LDH gel with the TiO_2 solid, causing fewer particles of the TiO_2 photocatalyst to remain on the external surface, instead of being diffused in the interior causing lower photodegradation rates [12].

3.2. Photodegradation and phenol adsorption tests

In heterogeneous photocatalysis processes, several phenomena can occur. Direct photodegradation is where the adsorption of the organic pollutant on the surface of the catalyst promotes its decomposition by the action of the photogenerated holes. On the other hand, indirect photodegradation is based on the generation of •OH radicals which react with the organic matter degrading it. Other processes that may occur in phenol photodegradation are direct photolysis due to the presence of UV irradiation and photooxidation by the action of UV radiation and the oxidizing agent, but without any involvement from the photocatalyst [19].

As observed in **Figure 7**, after 120 minutes of photolytic reaction, degradation of phenol reaches 11.0% (1.1 mg/L). Since there is no absorption or light dispersion by the presence of any solid, majority of the photon flux was used for the photolytic reaction. This process reaches higher speed during the first 30 minutes of irradiation, and then the rate of photodegradation decreases but without reaching equilibrium, attaining the lowest level in all tests due to the lack of a material to act as photocatalyst and/or adsorbent [37]. For precursor photocatalysts, phenol degradation rates of 38.2 (3.8 mg/L), 41.8 (4.2 mg/L), and 54.6% (5.5 g/L) were obtained for TiO_2T, TiO_2I, and TiO_2B, respectively, during 120 minutes of irradiation. Although the TiO_2 anatase phase predominates in all the photocatalysts, as shown in the DRX analysis, the higher performance of the TiO_2B sample is attributed to the anatase-rutile ratio of 88:12%, which is the closest to the optimal one (80:20%); the rutile phase acts as a e^-_{BC} collector reducing recombination rates with h^+_{BV} and transferring the pollutant particles to the active TiO_2 anatase phase [38]. Another important difference is observed in the formation of crystalline phases of TiO_2 without photocatalytic properties [39], finding the presence of monoclinical TiO and rhombohedral TiO_2 in the TiO_2T sample, while the TiO_2 brookite phase forms in TiO_2I, resulting in lower photocatalytic efficiency and in TiO_2B the anatase and rutile phases they are present.

In addition, based on the particle size obtained for these photocatalysts, it is known that the optimum size in a TiO_2 photocatalyst is in the range of 20 to 30 nm, since this gives an optimum balance between the production of e^-_{BC}-h^+_{BV} pairs and the recombination process due to the surface/volume ratio becoming larger, enabling the timely use of the photogenerated

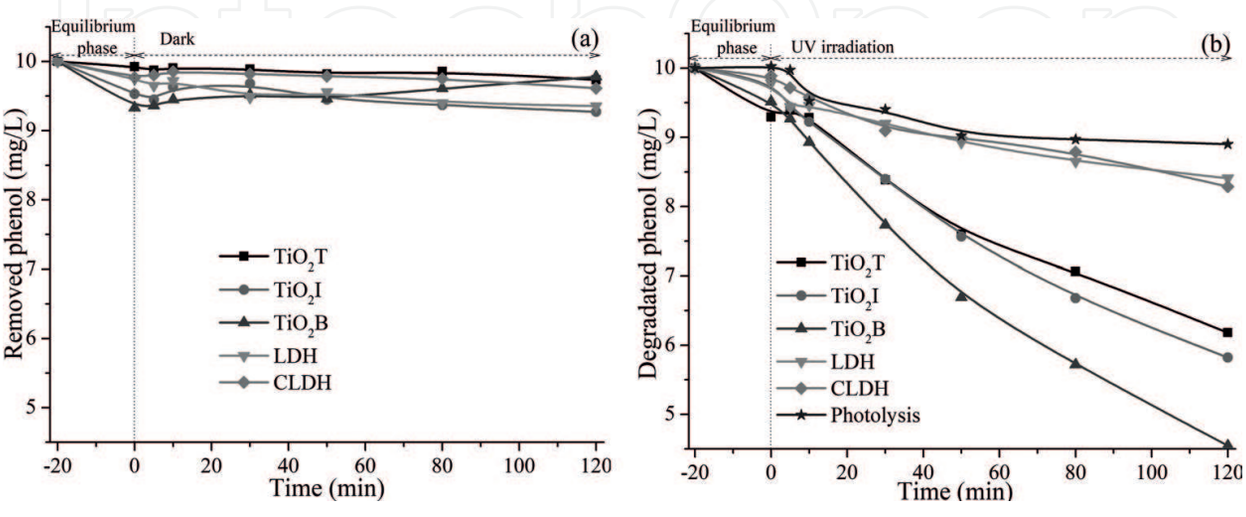

Figure 7. (a) Adsorption, (b) phenol photolysis, and photocatalytic degradation, with TiO_2 and LDH.

charges [39]. Considering the abovementioned, the particle size based on the AFM analysis is directly related to the percentage of photodegradation found in the photocatalysts, with the TiO_2T sample having the highest particle size (in the range of 35–175 nm), which is reflected in a lower photoactivity.

The adsorption rates found in the photocatalysts are lower and unrelated to the surface area of the materials, being slightly higher for TiO_2B (3.2%) 0.3 mg/L compared to TiO_2T (1.8%) and TiO_2I (1.5%), 0.2 and 0.1 mg/L, respectively. These results confirm the TiO_2B synthesis methodology as the most efficient for achieving maximum phenol degradation of 5.5 mg/L (54.6%). According to the XRD study, this is attributed mainly to the optimal anatase-rutile ratio of 88:12% and to smaller crystal size (25 nm), which is reflected in an optimal particle size range (15–50 nm), allowing e^-_{BC}-h^+_{BV} recombination to be minimized [40].

There is evidence that although LDH and CLDH are not semiconductors, these materials can act as photocatalysts since, due to the presence of Mg^{2+} and Al^{3+} cations, other materials with photoinduced defects on the oxide surface can be obtained, which can act as active centers for the surface reactions, promoting the generation of e^-_{BC}-h^+_{BV} pairs where the electron is delocalized toward the deficient charge of the Al^{3+} and the hole oxidizes the surrounding hydroxyl groups allowing the formation of •OH radicals [41, 30]. This statement is not reinforced by the results obtained in this study, where it can be observed (**Figure 7**) that the percentage of phenol degradation by photocatalysis for LDH and CLDH reaches 15.9 (1.6 mg/L) and 17.1%, (1.7 mg/L), respectively, after 120 minutes of irradiation. This behavior is mostly attributed to the concurrence of the adsorption and photolysis phenomena. Furthermore, in the adsorption process, lower percentages of phenol removal 3.9 (0.4 mg/L) and 2.7% (0.3 mg/L) were observed, with the value achieved with LDH being higher than with mixed oxides (CLDH), attributed to the greater surface area and pore volume of LDH.

The photodegradation curves obtained for the prepared composites are shown in **Figure 8**. It can be seen that the composites present higher phenol degradation rates than the LDH and CLDH precursors. The photodegradation curves in the composites show bigger photocatalytic activity during the first minutes of the reaction, when there is less competition between the phenol molecules to be degraded; as the passing of time, the photodegradation intermediates produced limit the elimination of phenol by the supported photocatalyst. Over time, there is no appreciable decrease in the photodegradation rate with the exception of the TiO_2B-LDH solid, where it can be observed that after the first few minutes of irradiation, the gradient of the curve remains stable, leading to higher percentages of phenol photodegradation. The formation of •OH radicals can be affected by excess coverage of LDH over the TiO_2 particles, causing a blocking of the radiant energy to the molecules of the photocatalyst [13]. The abovementioned is manifested mainly in the TiO_2T-LDH and TiO_2I-LDH samples, coinciding with the results of the AFM characterization.

The effect of synergy between a support material and a catalyst is based on the active surface exposed during the photocatalytic process [24, 36]. Higher degradation percentages were obtained for the TiO_2B-LDH sample, attributed to the methodology used in preparing the composite, which effectively reduces agglomeration and at the same time minimizes the screening phenomenon of the photocatalyst during UV irradiation. This is supported by the XPS results obtained, where it can be observed that the proportion of chemical interaction

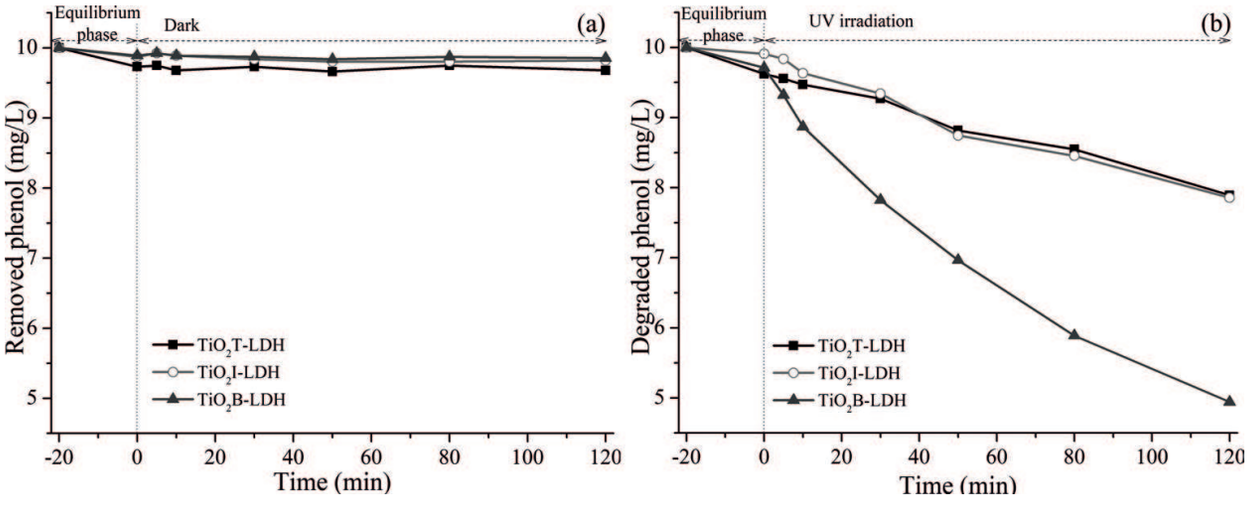

Figure 8. (a) Adsorption and (b) phenol photodegradation with TiO_2-LDH composites.

between Ti and mixed oxides (CLDH) is in direct relation to the photodegradation percentages, as observed for TiO_2T-LDH and TiO_2I-LDH, where there is a chemical interaction between Ti and the mixed oxides (CLDH), causing the impregnated Ti to be diffused to a greater degree inside the composite, with a lesser proportion to be spread over the surface [36]. The opposite can be seen in the TiO_2B-LDH sample, reflected in better photocatalytic performance.

Another possible cooperative effect between the TiO_2 mixed with LDH in the composites can be explained by the CLDH reconstruction process, since, when these are put in contact with an aqueous solution, they form highly hydroxylated species on the surface which can react with the photogenerated holes to promote •OH radical production, enabling them to attack the phenol more effectively [13].

The adsorptive capacity of the composites in general is minimal and is unrelated to the surface area of the materials; in the case of the TiO_2I-LDH sample, the percentage of phenol adsorbed is 1.5% (0.15 mg/L), in TiO_2T-LDH is 1.8% (0.18 mg/L), and in TiO_2B-LDH is 3.2% (0.32 mg/L).

Based on the results obtained, it can be assumed that, in general, phenol removal in the composites is attributed to indirect photocatalytic degradation through oxidation by •OH radicals as opposed to direct degradation by photogenerated holes due to the low adsorption rates of these materials [19].

The photocatalytic efficiency in the synthesized TiO_2-LDH composites depends mainly on the degree of chemical interaction of the impregnated Ti, which is in direct relation to the proportion of Ti diffused into the composite and the presence of photocatalytically active phases found on the surface of the material leaving the catalyst more exposed to UV irradiation, avoiding agglomeration and the screening phenomenon.

3.3. Evaluation of the photocatalyst concentration

Figure 9 shows photocatalytic performance in terms of the concentration of the solid (0.5, 1.0, 1.5, and 2 g/L) obtained with the composites. In photocatalysts with surface areas between 50

http://dx.doi.org/10.5772/intechopen.72279

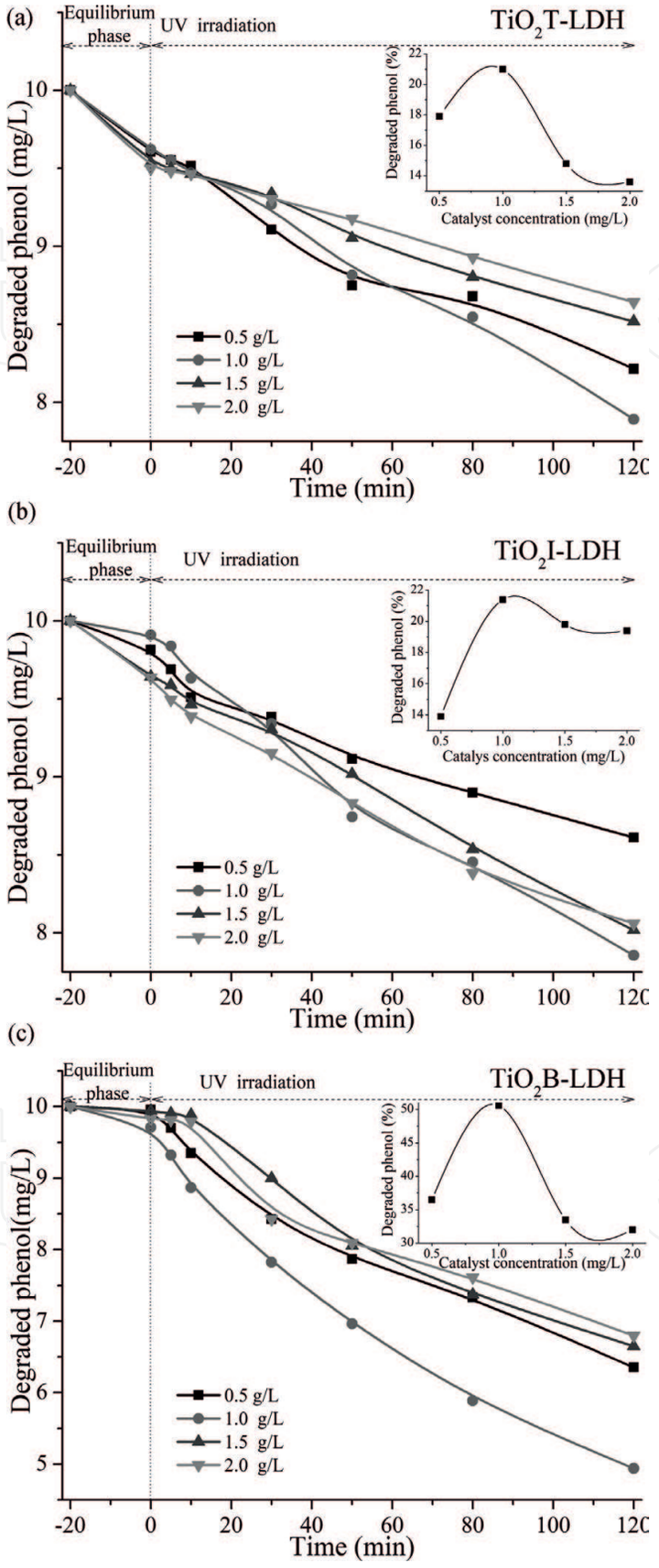

Figure 9. Composite concentration effect at photocatalytic yields.

and 200 m^2/g, the optimal concentration was found in the 0.5 to 3.0 g/L range depending on the chemical characteristics and techniques of the irradiation system [19].

High or low dosages of the photocatalyst may lead to a decrease in the reaction rate, so it is advisable to use the concentration of the photocatalyst near the point where its steady state is reached, i.e., the optimal concentration will correspond to the minimum quantity for which the maximum reaction is obtained, which is the highest proportion of material that remains exposed during radiation [19]. For all the composites, this state is observed at a concentration of 1 g/L where the highest performance is reached. In all the samples analyzed, it is observed that in quantities of 0.5 g/L a limiting effect occurs between the number of photocatalytic sites available for the reaction and the amount of phenol to degrade resulting in lower degradation rates [42]. When increasing the concentration of the photocatalyst, the radiation screening and dispersal phenomena—due to turbidity by the particles in suspension—gradually start to become significant, preventing the complete illumination of the solid due to the filtering effect of the excess particles, which mask part of the photosensitive surface. In addition, a bigger amount of the photocatalyst can lead to the deactivation of active molecules by particle collision [19], as observed in the composites on increasing the concentration to 2 g/L.

3.4. Phenol photodegradation in cycles with TiO_2-LDH composites

One advantage of using TiO_2 composites is their easy recovery and reuse over several degradation cycles [43]. The results obtained on reusing a single solid from the synthesized composites over four rounds are shown in **Figure 10**, indicating the percentage of photodegraded phenol in each cycle. This behavior is favorable for the composites, since they can be reused, thereby demonstrating the synergy between mixed oxides derived from CLDH and TiO_2, which, once they form the composite, cannot be separated and are therefore reusable.

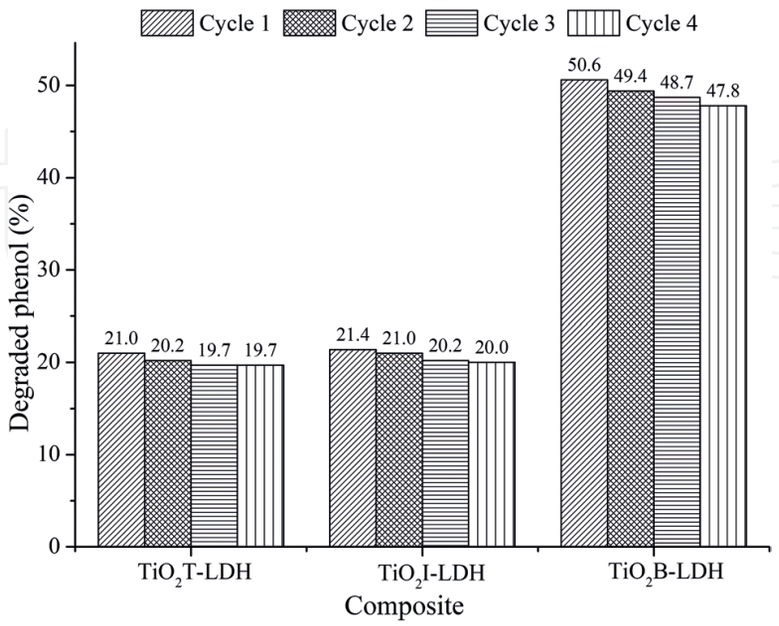

Figure 10. Phenol photodegradation using reutilized composites.

The results show that the photocatalytic capacity of the materials is maintained without further decreasing the degradation performance. The decline of photocatalytic activity in successive photodegradation cycles, in general, is not significant and is attributed to the gradual deactivation of the catalyst in the composites and, to a lesser extent, the minimum quantity of solid lost after the aliquot is taken and that cannot be recovered at the end of the irradiation cycle [19].

4. Conclusions

TiO_2-LDH composites were prepared from TiO_2 using three different methodologies, and LDHs were obtained by sol-gel synthesis, which are combined following different procedures. The different methodologies used to prepare the photocatalysts and the composites influence the photocatalytic activity of the materials, giving them different characteristics, being the most significant generation of mixed crystalline phases of TiO_2 with photocatalytic properties (anatase and rutile) in a ratio close to that reported as adequate (≈80:20%), the absence of TiO_2 phases without photocatalytic properties, and the particle size (between 15 and 50 nm), which allows an optimal balance between the production and recombination of photogenerated electron-hole pairs. The TiO_2B precursor was the photocatalyst whose characteristics were closest to those described to promote greater photocatalytic activity. The composites originate distinct forms of interaction between the components affecting their photoactivity. Based on the characterization results in the TiO_2T-LDH and TiO_2I-LDH composites, a bigger chemical interaction and larger crystals are observed, which indicates the degree of diffusion of TiO_2 inside the composite. Meanwhile, in the TiO_2B-LDH sample, the components remain segregated, with less chemical interaction, at the same time allowing minimal agglomeration and screening of the photocatalyst enhancing the photocatalytic mechanism. For the composites obtained, phenol elimination is attributed mainly to the degradation process through oxidation reactions produced by the formation of •OH radicals, finding a minimal adsorptive capacity in the materials. In the analysis of the different concentrations of material, a dosage of 1 g/L was the most efficient, exposing the maximum amount of the composite to UV irradiation. In addition, the composites can be separated after use in the aqueous solution, allowing them to be reused with minimal loss of photocatalytic activity between each cycle.

Author details

Juan C. Contreras-Ruiz[1], Sonia Martínez-Gallegos[1]*, Jose L. García-Rivas[1], Julio C. González-Juárez[1] and Eduardo Ordoñez[2]

*Address all correspondence to: soniazteca@hotmail.com

1 Technological Institute of Toluca, Metepec, México

2 Department of Chemistry, National Institute of Nuclear Research, Mexico City, México

References

[1] Busca G, Berardinelli S, Resini C, Arrighi L. Technologies for the removal of phenol from fluid streams: A short review of recent developments. Journal of Hazardous Materials. 2008;**160**:265-288

[2] Anwar DI, Mulyadi D. Synthesis of Fe-TiO_2 composite as a photocatalyst for degradation of methylene blue. Procedia Chemistry. 2015;**17**:49-54

[3] Ba-Abbad MM, Kadhum AAH, Mohamad AB, Takriff M, Sopian K. Photochemical oxidation of concentrated chlorophenols under direct solar radiation. International Journal of Electrochemical Science. 2012;**7**:4871-4888

[4] Bouberka Z, Benabbou KA, Khenifi A, Maschke U. Degradation by irradiation of an acid orange 7 on colloidal TiO_2/(LDHs). Journal of Photochemistry and Photobiology A: Chemistry. 2014;**275**:21-29

[5] Lin SH, Chiou CH, Chang CK, Juang RS. Photocatalytic degradation of phenol on different phases of TiO_2 particles in aqueous suspensions under UV irradiation. Journal of Environmental Management. 2011;**92**:3098-3104

[6] Hoffmann MR, Martin ST, Choi W, Bahnemann DW. Environmental applications of semiconductor Photocatalysis. Chemical Reviews. 1995;**95**:69-96

[7] Linsebigler AL, Guangquan L, Yates JT. Photocatalysis on TiO_2 surfaces: Principles, mechanisms, and selected results. Chemical Reviews. 1995;**95**:735-758

[8] Yuangpho N, Le STT, Treerujiraphapong T, Khanitchaidecha W, Nakaruk A. Enhanced photocatalytic performance of TiO_2 particles via effect of anatase–rutile ratio. Physica E. 2015;**67**:18-22

[9] Zhou W, Pan K, Qu Y, Sun F, Tian C, Ren Z, Tian G, Photodegradation HF. Of organic contamination in wastewaters by bonding TiO_2/single-walled carbon nanotube composites with enhanced photocatalytic activity. Chemosphere. 2010;**81**:555-561

[10] Chong M, Vimonses V, Lei S, Jin B, Chow C, Saint C. Synthesis and characterization of novel titania impregnated kaolinite nano-photocatalyst. Microporous and Mesoporous Materials. 2009;**117**:233-242

[11] Vaccari A. Clays and catalysis: A promising future. Applied Clay Science. 1999:161-198

[12] Huang Z, Wua P, Lu Y, Wang X, Zhu N, Dang. Z. Enhancement of photocatalytic degradation of dimethyl phthalate with nano-TiO_2 immobilized onto hydrophobic layered double hydroxides: A mechanism study. Journal of Hazardous Materials. 2013;**246-247**: 70-78

[13] Paredes SP, Valenzuela MA, Fetter G, Flores SO. TiO_2/MgAl layered double hidroxides mechanical mixtures as efficient photocatalyst in phenol degradation. Journal of physics and Chemistry of solids. 2011;**72**:914-991

[14] Contreras-Ruiz J, Martínez-Gallegos S, Ordoñez E. Surface fractal dimension of composites TiO_2-hydrotalcite. Materials Characterization. 2016;**121**:17-22

[15] Contreras-Ruiz J, Martinez-Gallegos S, Ordoñez-Regil E, Gonzalez-Juarez J, Garcia-Rivas J. Synthesis of hydroxide–TiO2 compounds with photocatalytic activity for degradation of phenol. Journal of Electronic Materials. 2017;**46**(3):1658-1668

[16] Araña J, Peña A, Doña J, Colón G, Navio J, Pérez J. FTIR study of photocatalytic degradation of 2-propanol in gas phase with different TiO_2 catalysts. Applied Catalysis B: Environmental. 2009;**89**:204-213

[17] Valente J, Lima E, Toledo-Antonio J, Cortes-Jacome M, Lartundo-Rojas L, Montiel M, Prince J. Comprehending the thermal decomposition and reconstruction process of sol-gel MgAl layered double hydroxides. Journal of Physical Chemistry C. 2010;**114**:2089-2099

[18] González-Juárez JC, Jiménez-Becerril J, Carrasco-Ábrego H. Influence of pH on the degradation 4-chlorophenol by gamma radiocatalysis using SiO_2, Al_2O_3 and TiO_2. Journal of Radioanalytical and Nuclear Chemistry. 2008;**275**(2):257-260

[19] Kish H. On the problem of comparing rates or apparent quantum yields in heterogeneous photocatalysis. Angewandte Chemie International Edition. 2010;**49**:9588-9589

[20] Spurr RA, Myers H. Quantitative analysis of anatase rutile mixtures with an X-ray diffractometer. Analytical Chemistry. 1957;**29**:760-762

[21] Mendoza-Damián G, Tzompantzi F, Mantilla A, Barrera A, Lartundo-Rojas L. Photocatalytic degradation of 2,4-dichlorophenol with MgAlTi mixedoxides catalysts obtained from layered double hydroxides. Journal of Hazardous Materials. 2013;**263**:67-72

[22] Li B, Yuan SL. Synthesis, characterization, and evaluation of TiMgAlCu mixed oxides as novel SO_x removal catalysts. Ceramics International. 2014;**40**:11559-11566

[23] Tzompantzi F, Mendoza-Damián G, Rico JL, Mantilla A. Enhanced photoactivity for the phenol mineralization on ZnAlLa mixed oxides prepared from calcined LDHs. Catalysis Today. 2014;**56**:220-222. 56-60

[24] Seftel EM, Niarchos M, Mitropoulos CMM, Vansant EF, Cool P. Photocatalytic removal of phenol and methylene-blue in aqueous media using TiO_2@LDH clay nanocomposites. Catalysis Today. 2015;**252**:120-127

[25] Petrović VV, Obradović S, Žorić A, Milošević H. Influence of synthesis parameters on electrical properties of sistems MgO-TiO_2. Contemporary Materials. II. 2011:51-54

[26] West AR. Solid State Chemistry and its Application. New York: Wiley; 1984

[27] Liu S, Yu J, Jaroniec M. Anatase TiO_2 with dominant high-energy {001} facets: Synthesis, properties, and applications. Chemistry of Materials. 2011;**23**:4085-4093

[28] Othman MR, Helwani Z, Martunus WJN. Fernando, synthetic hydrotalcites from different routes and their application as catalysts and gas adsorbents: A review. Applied Organometallic Chemistry. 2009;**23**:335-346

[29] Chubar N, Gerda V, Megantari O, Micušik M, Omastova M, Heister K, Man P, Fraissard J. Applications versus properties of mg–al layered double hydroxides provided by their syntheses methods: Alkoxide and alkoxide-frsol–gel syntheses and hydrothermal precipitation. Chemical Engineering Journal. 2013;**234**:284-299

[30] Jacome-Acatitla G, Tzompantzi F, Lopez-Gonzalez R, Garcia-Mendoza C, Alvaroa JM, Gomez R. Photodegradation of sodium naproxen and oxytetracycline hydrochloride in aqueous medium using as photocatalysts mg-al calcined hydrotalcites. Journal of Photochemistry and Photobiology A: Chemistry. 2014;**277**:82-89

[31] Peng F, Cai L, Huang L, Yu H, Wang H. Preparation of nitrogen-doped titanium dioxide with visible-light photocatalytic activity using a facile hydrothermal method. Journal of Physics and Chemistry of Solids. 2008;**69**(7):1657-1664

[32] Leprince-Wang Y. Study of the growth morphology of TiO_2 thin films by AFM and TEM. Surface and Coatings Technology. 2001;**140**:155-160

[33] Cedillo-Gonzalez EI, Montorsi M, Mugoni C, Montorsi M, Siligardi C. Improvement of the adhesion between TiO_2 nanofilm and glass substrate by roughness modifications. Physics Procedia. 2013;**40**:19-29

[34] Naumkin AV, Kraut-Vass A, Gaarenstroom SW, Powell CJ. NIST X-ray Photoelectron Spectroscopy Database NIST Standard Reference Database 20, Version 4.1 febrero 2016. [Online]. Available: http://srdata.nist.gov/. [Accessed: 2016]

[35] Kim LH, Kim K, Park S, Jeong YJ, Kim H, Chung DS, Kim SH, Park CE, Al_2O_3/TiO_2 nanolaminate thin film encapsulation for organic thin film transistors via plasma-enhanced atomic layer deposition. ACS Applied Materials & Interfaces. 2014;**6**:6731-6738

[36] Seftel EM, Mertens M, Cool P. The influence of the Ti^{4+} location on the formation of self-assembled nanocomposite systems based on TiO_2 and Mg/Al-LDHs with photocatalytic properties. Applied Catalysis B: Environmental. 2013. 134-135. 274-285

[37] Prince J, Tzompantzi F, Mendoza-Damián G, Hernández-Beltrán F, Valente JS. Photocatalytic degradation of phenol by semiconducting mixed oxides derived from Zn(Ga)al layered double hydroxides. Applied Catalysis B: Environmental. 2015;**163**:352-360

[38] Pino E, Encinas MV. Photocatalytic degradation of chlorophenols on TiO_2-325 mesh and TiO_2-P25. An extended kinetic study of photodegradation under competitive conditions. Journal of Photochemistry and Photobiology A: Chemistry. 2012;**242**:20-27

[39] Ahmad A, Hameed G, Aziz S. Syntesis and applications of TiO_2 nanoparticles. Engineering Advances. 2007;**1**:403-413

[40] Bayal N, Jeevanandam P. Synthesis of TiO_2_MgO mixed metal oxide nano particles via a sol_gel method and studies on their optical properties. Ceramics International. 2014;**40**:15463-15477

[41] Mantilla A, Jacome-Acatitla G, Morales-Mendoza G, Tzompantzi F, Gomez R. Degradation of 4-chlorophenol and p-cresol using MgAl hydrotalcite. Industrial & Engineering Chemistry Research. 2011;**50**:2762-2767

[42] Shaban YS, El Sayed MA, El Maradny AA, Al Farawati RK, Al Zobidi MI. Photocatalytic degradation of phenol in natural seawater using visible light active carbon modified (CM)-n-TiO_2 nanoparticles under UV light and natural sunlight illuminations. Chemosphere. 2013;**91**:307-313

[43] Bai X, Zhang X, Hua Z, Ma W, Dai Z, Huang X, Gu H. Uniformly distributed anatase TiO_2 nanoparticles on graphene: Synthesis, characterization, and photocatalytic application. Journal of Alloys and Compounds. 2014;**599**:10-18

IntechOpen